Applied Physics Letters

Waveguide-coupled heterodyne terahertz detector based on AlGaN/GaN high-electron-mobility transistor

Cite as: Appl. Phys. Lett. **121**, 081101 (2022); https://doi.org/10.1063/5.0095379
Submitted: 10 April 2022 • Accepted: 25 July 2022 • Published Online: 22 August 2022

Kaiqiang Zhu, Wei Feng, Yifan Zhu, et al.

AIP Publishing

Applied Physics Letters ARTICLE scitation.org/journal/apl

Waveguide-coupled heterodyne terahertz detector based on AlGaN/GaN high-electron-mobility transistor

Cite as: Appl. Phys. Lett. **121**, 081101 (2022); doi: 10.1063/5.0095379
Submitted: 10 April 2022 · Accepted: 25 July 2022 ·
Published Online: 22 August 2022

Kaiqiang Zhu,[1] Wei Feng,[2,3,4] Yifan Zhu,[2,3,4] Qingfeng Ding,[3,4,5] Yikun Wang,[1] Yu Xiao,[6,a)] Lin Jin,[3,4] Hua Qin,[2,3,4,5,a)] and Houjun Sun[1]

AFFILIATIONS

[1]Beijing Key Laboratory of Millimeter Wave and Terahertz Techniques, School of Integrated Circuits and Electronics, Beijing Institute of Technology, Beijing 100081, China
[2]School of Nano-Tech and Nano-Bionics, University of Science and Technology of China, Hefei 230026, China
[3]Key Laboratory of Nanodevices and Applications, Suzhou Institute of Nano-Tech and Nano-Bionics, Chinese Academy of Sciences, Suzhou 215123, China
[4]Key Laboratory of Nanodevices of Jiangsu Province, Suzhou 215123, China
[5]School of Physical Science and Technology, ShanghaiTech University, Shanghai 201210, China
[6]School of Electronics and Communication Engineering, Sun Yat-sen University, Guangzhou 510275, China

[a)]**Authors to whom correspondence should be addressed:** xiaoy283@mail.sysu.edu.cn and hqin2007@sinano.ac.cn

ABSTRACT

We report a room-temperature, low output impedance, broad intermediate-frequency (IF) bandwidth field-effect terahertz detector based on an AlGaN/GaN high-electron-mobility transistor (HEMT) integrated in a metal waveguide. The waveguide detector equips a pair of quasi-Yagi antenna probes that are used to couple the terahertz energy to the HEMT channel. The gate is configured as an asymmetric edge-coupled coplanar waveguide transmission line. This terahertz electric field is asymmetrically distributed in the channel along the edges of the transmission lines. The responsivity and noise for direct and heterodyne detections are characterized and analyzed at different local oscillator (LO) powers. The noise-equivalent power in direct detection is below 189 pW/Hz$^{1/2}$. Operated in a heterodyne mode with a LO power of −3 dBm, the detector offers a conversion loss less than 55 dB in a frequency band of 320–340 GHz. The channel in a form of transmission line performs the broad IF bandwidth, which is increased to gigahertz range (3 GHz), and reduces the output impedance to 377 Ω which is about 20 times lower than previously reported. The transmission-line impedance could be optimized together with the distribution of the terahertz electric field in the gated channel to reduce the conversion loss.

Terahertz (THz) radiation is generally defined as electromagnetic radiation typically associated with frequencies between 0.3 and 10 THz,[1] which can be detected by a number of different mechanisms, such as photothermoelectric,[2,3] photovoltaic,[4] Hall effect,[5] bolometric,[6,7] and plasma-wave rectification.[8–11] A heterodyne detector with low conversion loss (CL) in combination with a wideband intermediate-frequency (IF) bandwidth can meet the demand for long-range and high-resolution detections of radar or high-data rate communication. In a terahertz regime, the Schottky diode mixers are often used in heterodyne imaging systems, which have an IF bandwidth of greater than 4 GHz and a CL of lower than 8 dB.[12,13] In wireless systems, up to 3.25 GHz IF bandwidth will deliver data rates in excess of 10 Gb/s.[14,15] Among them, field-effect transistor (FET) detectors based on plasma-wave detection and Schottky barrier diode (SBD) detectors have great potential for applications at room temperature.[16–20] Waveguide-based and quasi-optical heterodyne detectors based on SBD with outstanding performance are commercially available.[21–23] There are no ready solutions for three-terminal transistors,[24] compared with SBDs which benefit from well-developed techniques for integration into a metal waveguide.[25] The three-terminal transistors contain source, gate, and drain. It is difficult for traditional transistor structures to be integrated with planar transmission lines in the

waveguide, such as a suspended microstrip line, while an asymmetrical electric field should be formed under the gate and a bias wire need to be bonded on the gate.

Antenna-coupled THz FET detectors operated in the subthreshold region usually have a high channel resistance resulting from low carrier density; meanwhile, the small channel width of the FET also contributes to the channel resistance. For all the reasons mentioned above, there is a high output impedance between the source and the drain. The IF bandwidth is limited by the high output impedance. A typical example previously reported is that the channel resistance for a quasi-optical detector with an integrated asymmetric dipole antenna reached up to 8 kΩ.[26] Another with an integrated broadband bow-tie antenna also had a high impedance of 7.6 kΩ.[27] There is approximately 40 times as much impedance mentioned as the characteristic impedance (50 Ω) of the standard radio frequency (RF) transmission system. For such a high impedance, impedance matching will be a major challenge.

Compared to heterodyne detection in quasi-optical configuration, waveguides can control electromagnetic (EM) wave propagation in a closed boundary,[28] providing a uniform distribution of signal and fixed energy propagation mode with high stability and miniaturized system integration.[29,30] Hence, a wide IF bandwidth and low output impedance waveguide-coupled THz heterodyne detector are highly desired.

In this Letter, we proposed a heterodyne terahertz waveguide-coupled high-electron mobility transistor (HEMT) detector. A prototype detector operated at around 340 GHz was fabricated, assembled, and characterized. This approach offers the possibility of integrating the HEMT detector into a metal waveguide and reducing the output impedance to increase the IF bandwidth.

The waveguide detector based on the AlGaN/GaN heterostructure was fabricated on a sapphire substrate with a thickness of 50 μm, which provides a two-dimensional electron gas (2DEG) about 25 nm below the surface. The mobility and density of electrons at room temperature are $\mu = 1880\ \mathrm{cm^2\ V^{-1}\ s^{-1}}$ and $n_s = 0.836 \times 10^{13}\ \mathrm{cm^{-2}}$ according to our previous work,[31] respectively.

Figure 1(a) provides an exploded view of the proposed waveguide detector, and Fig. 1(e) provides the schematic of the proposed waveguide detector. When operated in the heterodyne detection mode, the local oscillation (LO) signal and the RF signal are fed, respectively, from the two waveguide ports, Waveguide Port 1 (WP1) and Waveguide Port 2 (WP2), as shown in Figs. 1(b) and 1(e).

The quasi-Yagi antenna probes are inserted into the E-plane of the metal WR-2.8 waveguides and consist of three elements (one dipole antenna as a driven element, one reflector, and one director), as shown in Fig. 1(e). Figure 1(c) shows the micrograph of the proposed detector. To enhance the electric field (E-field) under the gate, an asymmetric edge-coupled coplanar waveguide (CCPW) with two parallel coupled strip conductors asymmetrically located between the drain and the source ohmic contacts was chosen to transmit the EM wave above the HEMT channel. Additionally, a carefully designed tapered coupled microstrip line makes a transition between the quasi-Yagi antenna probe and the CCPW to optimize impedance matching for broadband performance. The design allows the THz energy to be coupled by the quasi-Yagi antenna probes and partially coupled into the active mixing region. The active mixing region is where the 2DEG is controlled by V_{gs} below the gate. Furthermore, low-pass compact microstrip resonant cell (CMRC) filters are applied to reduce the leakage of the THz signal from the CCPW. The proposed CMRC filter offers a wide stopband with 15 dB from 320–350 GHz and has a −3 dB passband bandwidth from 0 to 8 GHz.

The schematic of the AlGaN/GaN HEMT used in the waveguide detector is shown in Fig. 2(a). The mode of propagation along the transmission lines (TL) is the quasi-transverse electromagnetic (quasi-TEM) mode and supports two modes: even-mode and odd-mode.[32] In odd-mode excitation, the currents on the two parallel coupled strip conductors have the same magnitude with 180° out-of-phase, while even-mode delineates equal and in-phase. When the TL is driven in the odd-mode by the quasi-Yagi antenna probes, the E-field distributions are illustrated in Fig. 2(a) with purple lines. One of the two parallel coupled strip conductors, which is close to the source, is directly connected to the gate voltage source, so a voltage V_{gs} can be applied to the gate, termed "Gate line." Meanwhile, another strip conductor is defined as "Float line."

Figure 2(b) shows the equivalent circuit of the AlGaN/GaN HEMT mentioned above. Upon the incident THz power P_0, the amplitude of the E-field at the waveguide port E_0, the horizontal ($E_x = \dot{\xi}_x E_0 \cos \omega t$), and the perpendicular [$E_z = \dot{\xi}_z E_0 \cos(\omega t + \phi)$] E-fields are induced in the gated channel, where $\dot{\xi}_x$, $\dot{\xi}_z$ and ϕ are the horizontal and perpendicular enhancement factors and the phase difference between the two induced fields, respectively. The photoresponse is generated by the waveguide detector and absorbed by the amplifier in a form of photovoltage v_{ds} as[33–35]

$$v_{ds} = \frac{r_{amp}}{1 + (r_s + r_d + r_{amp})G_{ds}} i_0 = \frac{r_{amp}}{1 + (r_s + r_d + r_{amp})G_{ds}} \frac{dG_{ds}}{dV_{gs}} \int_0^L Z_0 P_0 \dot{\xi}_x \dot{\xi}_z \cos\phi \bar{z}\, dx, \quad (1)$$

where i_0 and $G_{ds} = \int_0^L G_0 dx = 1/r_{ds}$ are the mixing photocurrent and the conductance of the gated channel, respectively; r_s and r_d are the series resistances of the source/drain lead; and r_{amp} is the input impedance of the voltage amplifier. The integral in Eq. (1) represents the overall mixing factor Λ. According to Eq. (1), when ϕ is unequal to $\pm\pi/2$, the photovoltage v_{ds} could be measured. The asymmetric structure ($S_{c1} > S_{c3}$) is a key feature to achieve the strength of the E-field between the gate and the sources being greater than on the other side, which causes most of the EM-field energy to propagate near Gate line.

For small drain voltages, the channel resistance is given by[36]

$$r_{ds} \approx \frac{L_{ch}}{W_{ch}} \frac{1}{\mu_n C_0 (V_{gs} - V_{TH})}, \quad (2)$$

where W_{ch} and L_{ch} correspond to the width and length of the transistor channel, μ_n is the electron mobility in the channel, C_0 represents the capacitance introduced by 2DEG, and V_{TH} is the threshold voltage. Compared to our previous work, DET-200,[37] L_{ch} has increased from 0.3 to 0.9 μm, and W_{ch} has increased from 5 to 150 μm. The impedance r_{ds} of the proposed detector is expected to be reduced to at least 1/10 of the previously reported quasi-optical detector design.

The detector is based on plasma wave rectification detection. The principle behind this phenomenon was discovered by Dyakonov and Shur.[8,38] The plasmon waves can be excited from source either resonantly or nonresonantly by THz wave in the HEMT channel.[39] The proposed detector has a long gate, whose length of gate L_{ch} is 0.9 μm.

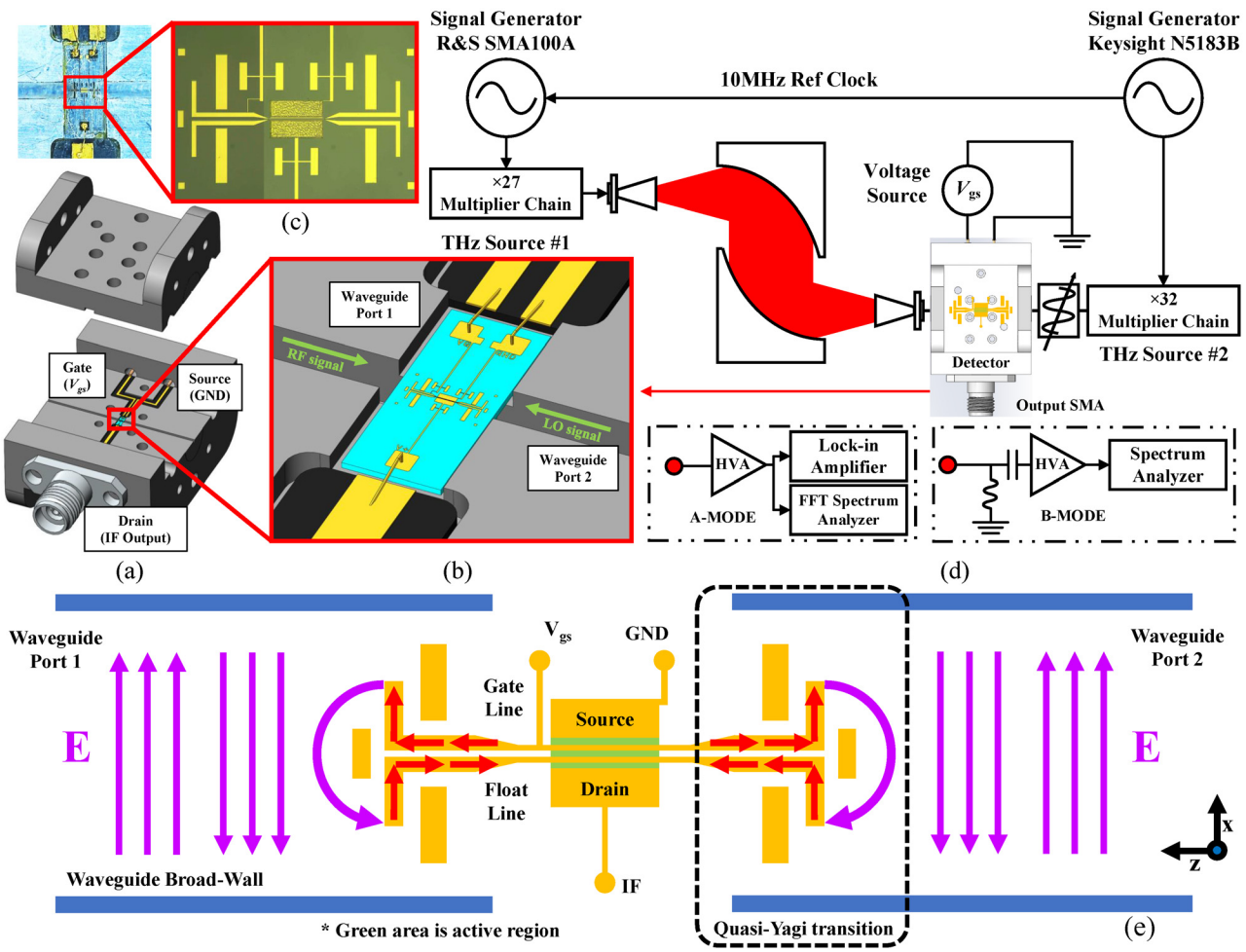

FIG. 1. (a) The exploded view of the proposed waveguide detector. (b) Configuration of the proposed waveguide detector. (c) The micrograph of the proposed waveguide detector. (d) Measurement setup for the proposed waveguide detector. (e) The schematic of the proposed waveguide detector.

The plasma waves will decay before reaching the drain contact. Given the relative low mobility of electrons in AlGaN/GaN at room temperature, the plasma waves are overdamped, and even other HEMT materials with higher mobility of electrons cannot reach resonant behavior at room temperature in this long gate. Therefore, the device operates in the non-resonant mode. This TL configuration guarantees that the incident terahertz wave induces an asymmetric E-field distribution under Gate line and around the 2DEG. This asymmetric E-field modulates the electron density and the velocity at the same time and drives electrons to the edges of the HEMT channel. The asymmetric structure of the TL induces the net electrons traveling in the HEMT channel from the source to the drain. The coordinate origin is located at the symmetric center point between *Float line* and Gate line. Figures 3(a) and 3(b) provide the intensities of the E-field (E_x and E_z), the simulated spatial distributions of the mixing factor Λ, and the phase difference. This asymmetry of induced E-field produces an unbalanced mixing factor Λ between the two edges of the Gate line, which drives electrons in 2DEG to produce photoresponse. Figure 3(c) shows the spatial distributions of the mixing factor Λ. The simulation results are from the commercial software HFSS with a THz signal ($P_{in} = 1$ W, initial phase = 90°, $f_0 = 340$ GHz) fed by WP1. When the mixing factor Λ is combined along Gate line, the mixing factor Λ value reached 4000 a.u. As Fig. 3(c) depicted, there are nearly 2/3 of the active mixing region of values greater than half of the maximum mixing factor Λ, which indicates producing the relatively strong photoresponse, which shows that the detector responds to terahertz signals efficiently.

The S-parameters of the waveguide detector are characterized by a Rohde & Schwarz ZVA50 VNA analyzer with ZC500 extension units, and the results are provided in the supplementary material. For this detector, isolation can reflect the absorption of the THz radiation power by 2DEG. The gate voltage V_{gs} adjusts the 2DEG concentration, as the depletion mode HEMT. A more negative gate voltage causes a lower 2DEG concentration, which means that the |S21| and |S12| will gradually increase. The coefficient of EM energy dissipated in the detector can be approximated as

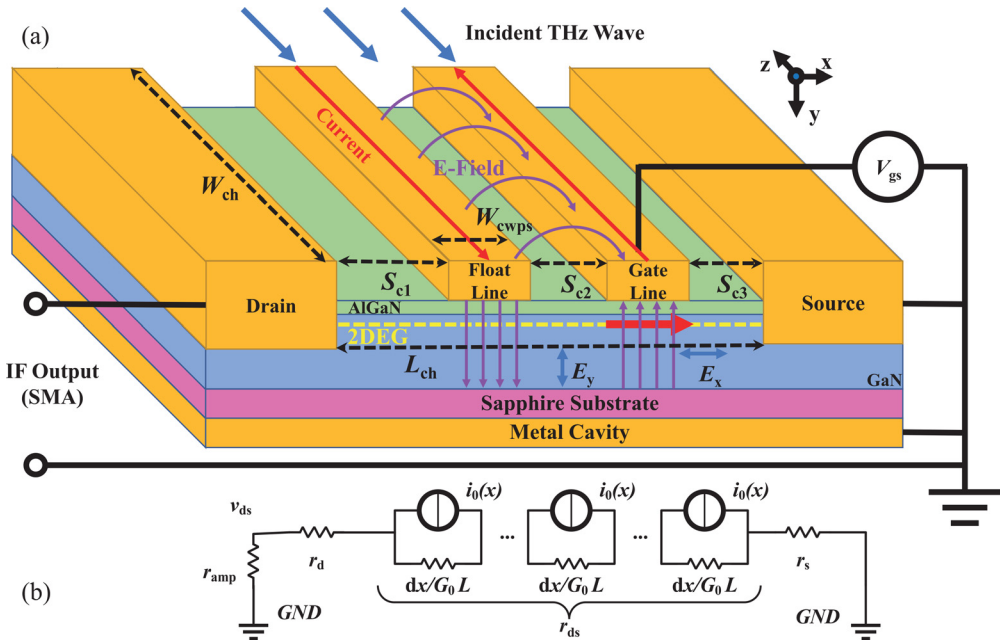

FIG. 2. Schematic and equivalent circuit of the AlGaN/GaN transistor, used in the proposed waveguide detector.

$$\alpha_{\text{dissipated-Port1}} = \frac{P_{\text{dissipated}}}{P_{\text{incident}}} = 1 - |S11|^2 - |S21|^2. \quad (3)$$

Calculation from the measured S-parameters shows that about 90% of the energy is dissipated in the detector at the $V_{gs} = -4$ and -4.2 V. Although not all of this THz EM energy is used efficiently to excite the photoresponse, the HEMT structures with higher coupling efficiency have greater potential for higher responsivity.

Figure 1(d) shows the experimental setup to characterize the performance of direct and heterodyne modes. RF and LO THz signals near 340 GHz are generated by two independent frequency multiplier chains, driven by separate signal generators. The two signal generators are synchronized by a 10 MHz reference clock. THz source #1 radiates RF THz signals through diagonal horn antennas, and two off axis parabolic mirrors focus the THz RF beam on the detector through a diagonal horn as above. The 3 dB beam width of the mentioned diagonal

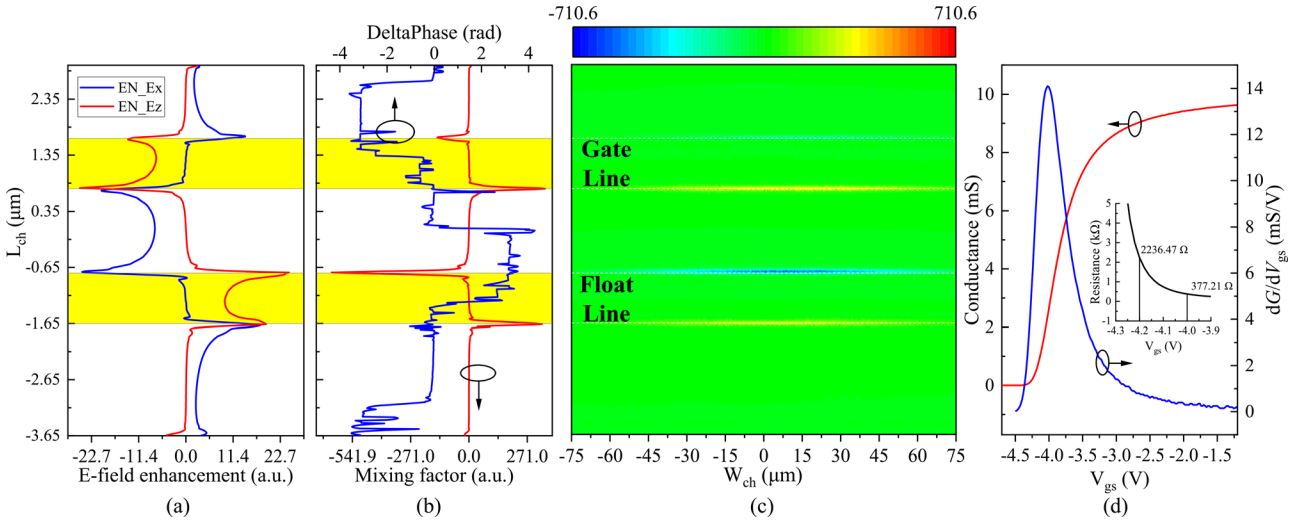

FIG. 3. (a) Distribution of the induced electric fields (E_x and E_z) between the source and drain, along the line at HEMT's center ($W_{ch} = 0$). (b) Distribution of the mixing factor Λ and phase shift (ϕ) between E_x and E_z on the abovementioned condition. (c) A color-scale 2D plot of the spatial distribution of the mixing factor Λ. (d) The resistance, conductance, and dG_{ds}/dV_{gs} of the detector as a function of V_{gs} at $V_{ds} = 10$ mV.

horns is 22° with an aperture of $6 \times 6\,\text{mm}^2$. THz source #2 provides LO signals to the detector through a metal WR-2.8 waveguide. A tunable WR-2.8 attenuator (CMi VA2.8R) is inserted between the detector and THz source #2 to adjust the LO power. The power of both sources at different frequencies is calibrated by a THz power meter (VDI Erickson PM5B).

In a direct mode measurement, an A-MODE readout circuit, including a voltage amplifier (FEMTO HVA-200M-40-B), is connected to the detector's output port. The bandwidth and gain of the voltage amplifier are 200 MHz and 40 dB, respectively, with a low input noise of 1.2 $\text{nV/Hz}^{1/2}$. The THz source is amplitude modulated by an 11.117 kHz square-wave with a duty cycle of 50%. In addition, a lock-in amplifier (Signal Recovery Model 7265) is used to measure v_{ds}, and a fast Fourier transform spectrum analyzer (Stanford Research SR770) is used to record the noise.

For an I–V measurement, the drain was biased to a small voltage from 0 to 10 mV and the source was grounded and the gate was biased to a specific gate voltage. Figure 3(d) shows the results of the source–drain conductance and the differential conductance tuned by the gate voltage. The inset of Fig. 3(d) depicts the source–drain resistance. To characterize the two input ports in a direct detection mode, the two THz sources were turned on separately. The optimal sensitivities for both input waveguide ports are found to be located at the gate voltage of −4.2 V which are determined by the simultaneously measured total noise level and the voltage responsivity. The typical detector responsivity is 20.0 V/W for WP1 and 43.8 V/W for WP2, as shown in Fig. 4(a). Meanwhile, the average noise-equivalent power (NEP) amounts to 422 $\text{pW/Hz}^{1/2}$ for WP1 and 189 $\text{pW/Hz}^{1/2}$ for WP2, as shown in Fig. 4(b). The difference in sensitivities and NEP of two waveguide ports is the result of a sequence assembly error. The lowest NEP (81 $\text{pW/Hz}^{1/2}$) of the proposed waveguide detector is about 22 times as large as the value of 3.7 $\text{pW/Hz}^{1/2}$ of our previous proposed quasi-optical detectors.[26,37] And at the optimal gate voltage ($V_{gs} = -4.20$ V), measured total noise mainly caused by thermal noise from the waveguide detector is 9.35 $\text{nV/Hz}^{1/2}$, and the channel resistance is 2.23 kΩ, as shown in Fig. 3(d), which is about one fourth compared to the detector recently reported by Feng *et al.*[26] with an internal impedance of 8 kΩ.

In the heterodyne mode measurement, the B-MODE readout circuit is connected to the output port. The two signal generators generate different frequency signals, which are multiplied to produce LO ($f_{LO} = 32 \times f_{mw1}$) and RF signals ($f_{RF} = 27 \times f_{mw2}$) with frequency differences ($\Delta f = |f_{LO} - f_{RF}|$). A bias-tee (Picosecond Model 5550B) is used to remove the DC produced by the strong LO signal and to couple out the IF signal and the noise from the drain, both of which are amplified with a low-noise voltage amplifier and measured by a spectrum analyzer (Tektronix RS306B).

The IF power is measured as a function of the gate voltage at a fixed IF frequency ($\Delta f = 51.3$ MHz), as shown in Figs. 4(c) and 4(d). In this situation, the RF power (P_{RF}) is set at about 2 μW (−27 dBm), and the LO power ranges from −23.1 to 11.8 dBm. The optimal gate voltage for the maximum IF signal power is fixed at −4.00 V and the channel resistance is 377.2 Ω.

To obtain the maximum bandwidth of the IF signal, an RF amplifier is chosen to replace the FEMTO voltage amplifier which has only 200 MHz operating bandwidth. The gain and operating bandwidth of the RF amplifier are 40 dB and 2.0 GHz, respectively. Since the input impedance of the RF amplifier is 50 Ω, an insertion loss about 3.8 dB comes from the impedance mismatching. The LO frequency is set at 320 GHz, and the RF frequency is changed from 320 to 323 GHz with 27 MHz intervals. Meanwhile, the IF signals and the noise spectrum are recorded by a spectrum analyzer (Tektronix RS306B), simultaneously.

Figure 5(a) shows the IF signal power and noise at different IF frequencies. The signal-to-noise ratio (SNR) and conversion loss (CL) are defined as $\text{SNR(dB)} = P_{IF}(\text{dBm}) - N_{IF}(\text{dBm})$ and $\text{CL(dB)} = P_{RF}(\text{dBm}) - P_{IF}(\text{dBm}) + G_{AMP}(\text{dB})$, respectively. When the IF frequency reaches gigahertz frequencies, the IF noise increases rapidly with increasing P_{LO} and starts to increase slowly when the LO power reaches 5.8 dBm, as shown in Fig. 5(a). A strong LO signal will drive the detector to saturation. The IF signal and noise will be suppressed as a result of the electron accumulation in the channel. While SNR

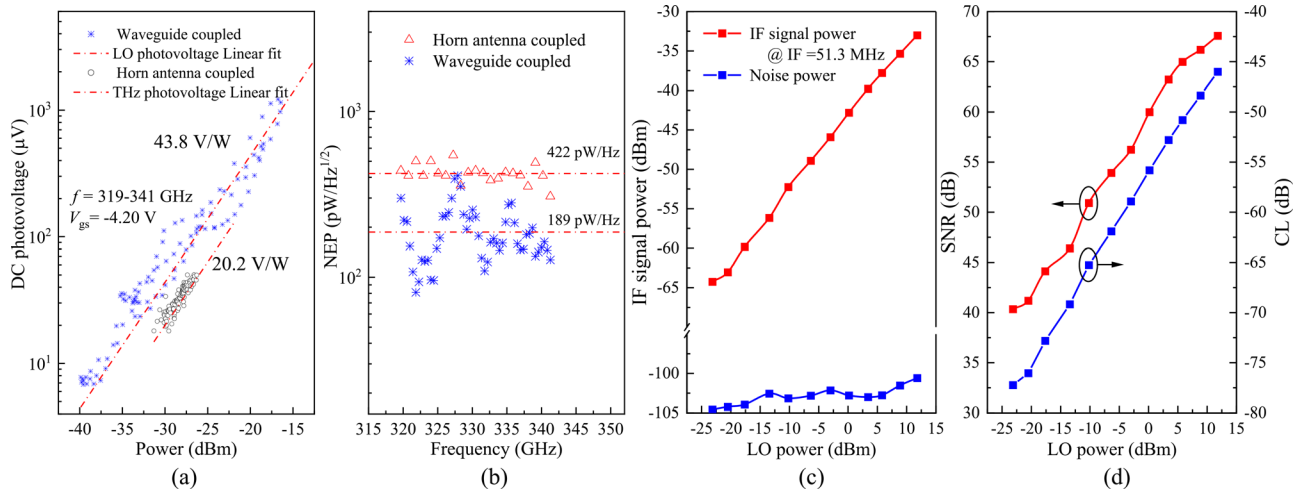

FIG. 4. (a) The DC photovoltage from direct detection for two input waveguide ports of a proposed detector. The dashed line is the fit for the measured data. (b) The NEP for two input waveguide ports of a proposed detector in direct detection. (c) Measured IF signal (red line) and noise power (blue line) at different LO powers. (d) Calculated SNR (red line) and CL (blue line) at different LO power levels based on IF signal power, noise level, and RF signal power in the heterodyne mode.

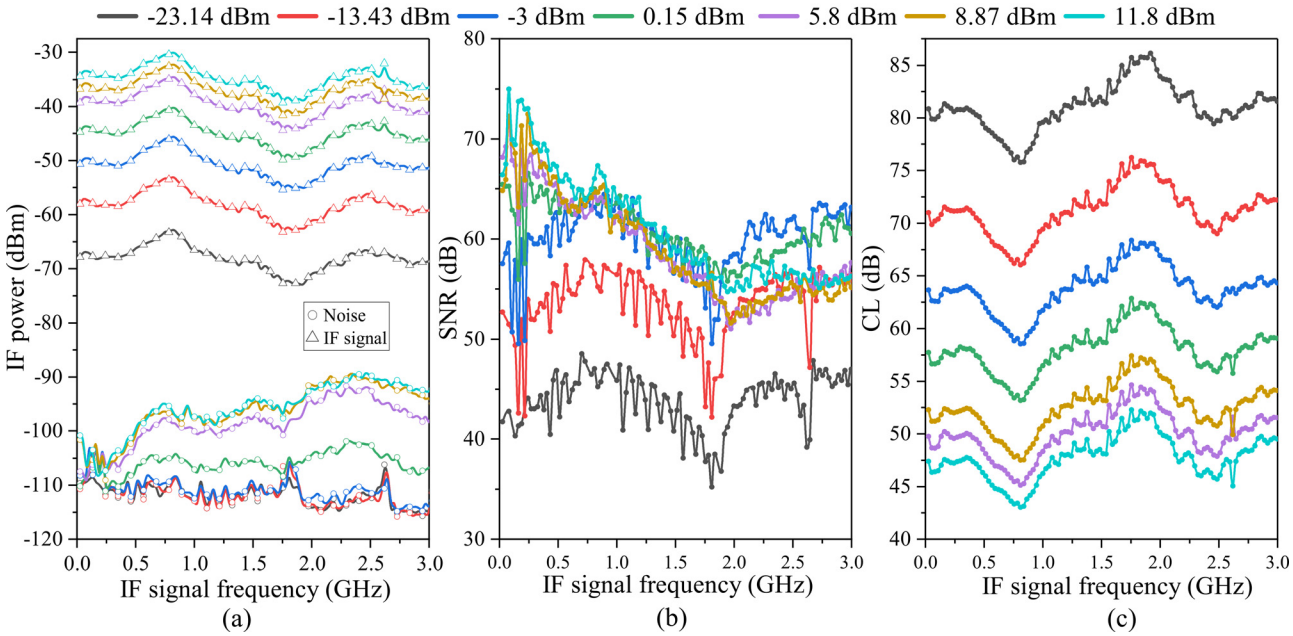

FIG. 5. (a) Measured IF signal and noise at different LO powers. (b) Calculated SNR at different LO powers. (c) Calculated CL at different LO powers.

does not increase with increasing LO power, when the LO power is greater than −3 dBm, as a result of the nonlinear growth of the IF noise in contrast to IF signal power. The IF bandwidth reached 3 GHz with SNR > 55 dB at $P_{LO} = -3$ dBm. For the LO power as stated above, we calculate the average heterodyne NEP (NEP $= P_{RF} - \mathrm{SNR} - 10\lg B$) to be −106 dBm/Hz or 25 fW/Hz, with IF frequency from 27 to 3024 MHz. There is a significant improvement in the IF bandwidth, compared to our previous heterodyne detector, which is only tens of megahertz.[26]

In conclusion, we have designed and characterized a waveguide heterodyne AlGaN/GaN HEMT detector equipped with two quasi-Yagi antenna probes and utilized CCPW as HEMT electrodes, fabricated on a sapphire substrate. The detector offers a NEP below 189 pW/Hz$^{1/2}$ around 340 GHz at room temperature in direct detection, the IF bandwidth exceeding 3 GHz and the conversion loss and isolation are about 55 and 15 dB with −3 dBm LO power in heterodyne detection, respectively. Compared to the quasi-optical FET detectors, this is an encouraging work that addresses possible solutions to reduce the output impedance, increase the IF bandwidth, and integrate HEMT into the metal waveguide. To meet the need for integration of the imaging or communication system, waveguide detectors need to be further developed to improve performance. It is undoubtedly that the noise and conversion loss must be further improved. The lower noise represents the better NEP. The high frequency noise mainly includes the thermal noise and the shot noise. Thermal noise comes from channel resistance and series resistance, which could be reduced by reducing all-in resistance. Using a wider gate width and a smaller gate length or utilizing materials with higher carrier mobility, such as graphene, could minimize all-in resistance. The shot noise is due to a DC from the self-mixing between the source and the drain. Passing inverse DC between the source and drain could significantly reduce the shot noise and increase the responsivity.[40] Also, the detector structure needs to be improved. The induced THz E-fields under gate decide the mixing factor. By optimizing the modulation of the above E-fields, the mixing factor could be increased to decrease the CL by enhancing the responsivity. The materials with higher carrier mobility could also contribute to decreasing CL. It is noteworthy that the shape of the detector chip has to be optimized. The proposed prototype is very difficult to assemble, and the assembly errors seriously affect the performance in the THz regime. Definitely, error-insensitive structures are a better choice.

See the supplementary material for more dimension details of the design and simulation results of the proposed detector. In addition, the measured S-parameters curves with different V_{gs} between 0 V and −5 V are provided.

The authors would like to thank Shixiong Liang from the National Key Laboratory of ASIC, Hebei Semiconductor Research Institute for his helpful advice on various technical issues examined in this Letter. The authors acknowledge the support from the National Natural Science Foundation of China (Nos. 62001522 and 61975227) and the Shenzhen Science and Technology Program (No. KQTD20190929172704911).

AUTHOR DECLARATIONS

Conflict of Interest

The authors have no conflicts to disclose.

Author Contributions

K.Z. and W.F. contributed equally to this work.

Kaiqiang Zhu: Conceptualization (equal); Data curation (equal); Formal analysis (equal); Investigation (equal); Methodology (lead); Validation (equal); Visualization (lead); Writing – original draft (lead); Writing – review & editing (lead). **Wei Feng:** Data curation (equal); Formal analysis (equal); Methodology (equal); Resources (equal); Validation (equal); Writing – original draft (equal); Writing – review & editing (equal). **Yifan Zhu:** Methodology (equal); Resources (equal); Validation (equal). **Qingfeng Ding:** Data curation (equal); Resources (equal). **Yikun Wang:** Formal analysis (equal); Investigation (equal). **Yu Xiao:** Conceptualization (equal); Formal analysis (equal); Investigation (equal); Methodology (equal); Supervision (equal); Writing – review & editing (equal). **Lin Jin:** Investigation (equal); Resources (equal); Visualization (equal). **Hua Qin:** Conceptualization (equal); Formal analysis (equal); Investigation (equal); Methodology (equal); Resources (equal); Supervision (lead); Writing – review & editing (equal). **Houjun Sun:** Investigation (equal); Resources (equal); Supervision (equal); Writing – review & editing (equal).

DATA AVAILABILITY

The data that support the findings of this study are available from the corresponding authors upon reasonable request.

REFERENCES

[1]H. Sarieddeen, M.-S. Alouini, and T. Y. Al-Naffouri, Proc. IEEE **109**, 1628 (2021).
[2]H. Ahmad, D. Suzuki, and Y. Kawano, AIP Adv. **8**, 115002 (2018).
[3]J. Bai, Z. Pang, P. Shen, T. Chen, W. Shen, S. Wang, and S. Chang, Opt. Commun. **497**, 127184 (2021).
[4]C. Somma, K. Reimann, C. Flytzanis, T. Elsaesser, and M. Woerner, Phys. Rev. Lett. **112**, 146602 (2014).
[5]T. Matsuda, N. Kanda, T. Higo, N. P. Armitage, S. Nakatsuji, and R. Matsunaga, Nat. Commun. **11**, 909 (2020).
[6]L. Vicarelli, A. Tredicucci, and A. Pitanti, ACS Photonics **9**, 360 (2022).
[7]Y. Zhang, X. Wang, Y. Zhou, H. Lai, P. Liu, H. Chen, X. Wang, and W. Xie, Nano Lett. **22**, 485 (2022).
[8]M. Dyakonov and M. Shur, IEEE Trans. Electron Devices **43**, 1640 (1996).
[9]E. Öjefors, A. Lisauskas, D. Glaab, H. G. Roskos, and U. R. Pfeiffer, J. Infrared, Millimeter, Terahertz Waves **30**, 1269–1280 (2009).
[10]F. Bianco, V. Mišeikis, D. Perenzoni, C. Coletti, M. Perenzoni, and A. Tredicucci, IEEE Trans. Terahertz Sci. Technol. **11**, 70 (2021).
[11]F. H. L. Koppens, T. Mueller, P. Avouris, A. C. Ferrari, M. S. Vitiello, and M. Polini, Nat. Nanotechnol. **9**, 780 (2014).
[12]S. R. Kasjoo, M. B. M. Mokhar, N. F. Zakaria, and N. J. Juhari, "A brief overview of detectors used for terahertz imaging systems," AIP Conf. Proc. **2203**, 020020 (2020).
[13]P. H. Siegel and R. J. Dengler, Int. J. Infrared Millimeter Waves **27**, 465 (2006).
[14]H. Tataria, M. Shafi, A. F. Molisch, M. Dohler, H. Sjoland, and F. Tufvesson, Proc. IEEE **109**, 1166 (2021).
[15]A. Goldsmith, *Wireless Communications* (Cambridge University Press, 2005).
[16]I. Gayduchenko, S. G. Xu, G. Alymov, M. Moskotin, I. Tretyakov, T. Taniguchi, K. Watanabe, G. Goltsman, A. K. Geim, G. Fedorov, D. Svintsov, and D. A. Bandurin, Nat. Commun. **12**, 543 (2021).
[17]I. Novodchuk, M. Bajcsy, and M. Yavuz, Carbon **172**, 431 (2021).
[18]I. V. Minin, O. V. Minin, J. Salvador-Sánchez, J. A. Delgado-Notario, J. A. Delgado-Notario, J. Calvo-Gallego, M. Ferrando-Bataller, K. Fobelets, J. E. Velázquez-Pérez, and Y. M. Meziani, Opt. Lett. **46**, 3061 (2021).
[19]S. van Berkel, E. S. Malotaux, C. de Martino, M. Spirito, D. Cavallo, A. Neto, and N. Llombart, IEEE Trans. Terahertz Sci. Technol. **11**, 495 (2021).
[20]A. Soni and M. Shrivastava, IEEE Trans. Electron Devices **68**, 2196 (2021).
[21]See https://www.vadiodes.com/en/products-6/detectors for "Virginia Diodes, Inc—Detectors," (2022).
[22]See https://www.vadiodes.com/en/products-6/mixers-shm-ehm-and-fm for "Virginia Diodes, Inc—Mixers," (2022).
[23]See https://acst.de/products/quasi-optical-detectors/ for "ACST GmbH—Quasi-Optical Detector," (2022).
[24]E. Javadi, D. B. But, K. Ikamas, J. Zdanevičius, W. Knap, and A. Lisauskas, Sensors **21**, 2909 (2021).
[25]T.-H. Ren, Y. Zhang, B. Yan, R.-M. Xu, C.-Y. Yang, J.-T. Zhou, and Z. Jin, Chin. Phys. Lett. **33**, 060701 (2016).
[26]W. Feng, Y. Zhu, Q. Ding, K. Zhu, J. Sun, J. Zhang, X. Li, Y. Shangguan, L. Jin, and H. Qin, Appl. Phys. Lett. **120**, 051103 (2022).
[27]M. Bauer, A. Ramer, S. A. Chevtchenko, K. Y. Osipov, D. Cibiraite, S. Pralgauskaite, K. Ikamas, A. Lisauskas, W. Heinrich, V. Krozer, and H. G. Roskos, IEEE Trans. Terahertz Sci. Technol. **9**, 430 (2019).
[28]Y. J. Cheng, W. Hong, and K. Wu, IEEE Trans. Antennas Propag. **56**, 3055 (2008).
[29]S. Atakaramians, S. Afshar V, T. M. Monro, and D. Abbott, Adv. Opt. Photonics **5**, 169 (2013).
[30]D. M. Pozar, *Microwave Engineering*, 4th ed. (Wiley Global Education, 2011).
[31]Y. F. Sun, J. D. Sun, Y. Zhou, R. B. Tan, C. H. Zeng, W. Xue, H. Qin, B. S. Zhang, and D. M. Wu, Appl. Phys. Lett. **98**, 252103 (2011).
[32]R. Mongia, I. J. Bahl, P. Bhartia, and S. J. Hong, *RF and Microwave Coupled-Line Circuits* (Artech House, 2007).
[33]J. D. Sun, Y. F. Sun, D. M. Wu, Y. Cai, H. Qin, and B. S. Zhang, Appl. Phys. Lett. **100**, 013506 (2012).
[34]R. A. Lewis, Appl. Phys. Lett. **100**, 173513 (2012).
[35]J. Sun, Y. Zhu, W. Feng, Q. Ding, H. Qin, Y. Sun, Z. Zhang, X. Li, J. Zhang, X. Li, Y. Shangguan, and L. Jin, Opt. Express **28**, 4911 (2020).
[36]J.-P. Colinge and C. A. Colinge, *Physics of Semiconductor Devices* (Springer Science & Business Media, 2005).
[37]J. Sun, W. Feng, Q. Ding, Y. Zhu, Z. Zhang, X. Li, H. Qin, J. Zhang, X. Li, Y. Shangguan, L. Jin, Y. Sun, and V. V. Popov, Appl. Phys. Lett. **116**, 161109 (2020).
[38]M. Dyakonov and M. Shur, Phys. Rev. Lett. **71**, 2465 (1993).
[39]A. Lisauskas, U. Pfeiffer, E. Öjefors, P. H. Bolïvar, D. Glaab, and H. G. Roskos, J. Appl. Phys. **105**, 114511 (2009).
[40]B. Gershgorin, V. Kachorovskii, Y. Lvov, and M. Shur, Electron. Lett. **44**, 1036 (2008).